Magnetic and crystal structure of the compound $(Y, Ce)_2Sr_2(Cu, Fe)_3O_{8+y}$

Magnetic and crystal structure of the compound $(Y, Ce)_2Sr_2(Cu, Fe)_3O_{8+y}$

M Pissas†§, C Christides†, G Kallias†, D Niarchos† and R Sonntag‡∥

† Institute of Materials Science, *Demokritos* National Centre for Scientific Research, 153 10 Agia Paraskevi, Attiki, Greece
‡ Berlin Neutron Scattering Centre, Hahn–Meitner-Institut, Glienickerstrasse 100, D-14109 Berlin, Germany

Abstract. In this work, we have studied the crystal and magnetic structure of fully de-oxygenated $(Y, Ce)_2Sr_2(Cu, Fe)_3O_{8+y}$ using neutron powder diffraction data. Rietveld profile refinement confirmed the presence of removable oxygen y within the Cu(1) layers. While for the fully oxygenated sample the $I4/mmm$ space group describes the crystal structure adequately, for the deoxygenated sample the space group $Cmcm$ was found to be more appropriate. $Cmcm$ accounts for the disorder within the Cu(1) layers, which was also observed with Mössbauer spectroscopy. For the deoxygenated sample, magnetic peaks corresponding to three-dimensional antiferromagnetism were observed and were indexed with the propagation vector $k_1 = (\frac{1}{2}\frac{1}{2}0)$ from 2 up to 300 K.

1. Introduction

An interesting variation of the $YBa_2Cu_3O_y$ (123) family of compounds can be obtained by replacing the rare-earth layer with a fluorite-structured block. In this context, the homologous series $(Fe, Cu)Sr_2(Y, Ce)_nCu_2O_{4+2n+y}$ (12n2) have been synthesized by Wada *et al* [1]. The $n = 2$ member is derived from $CuSr_2YCu_2O_{6+y}$ (1212) by simultaneous substitution of an (Fe, Cu)O layer for the CuO layer and a fluorite-like $(Y, Ce)_2O_2$ lamella for the Y layer. The fluorite block increases the thickness of the neighbouring perovskite block and usually has negative charge ($[(Y^{3+}, Ce^{4+})O_2^{-2}]^{\delta-}$), thereby acting as an electron donor for the perovskite block. Consequently, the hole concentration in the CuO_2 planes decreases.

In a previous paper [2] we presented a study of a $Y_{1.5}Ce_{0.5}Sr_2Cu_2FeO_{8+y}$ sample using x-ray diffraction, dc magnetic susceptibility and Mössbauer data. Both Mössbauer and magnetic susceptibility revealed a magnetic transition near 360 K for the oxygen-reduced (OR) sample. The Mössbauer spectra in the paramagnetic region were consistently fitted [2, 3] with two sites, A_r and D_r. Component A_r corresponds to pyramidal Fe^{3+} ($S = 5/2$) located in the Cu(2) planes and component D_r to distorted tetrahedral Fe^{3+} ($S = 5/2$) located in the Cu(1) layer. It is well known that heavily Fe-doped deoxygenated 123 exhibits long-range magnetic order with both sublattices Cu(1) and Cu(2) being magnetically ordered. It is interesting to examine whether the present compound exhibits long-range magnetic

§ E-mail address: mpissas@artemis.ims.ariadne-t.gr.
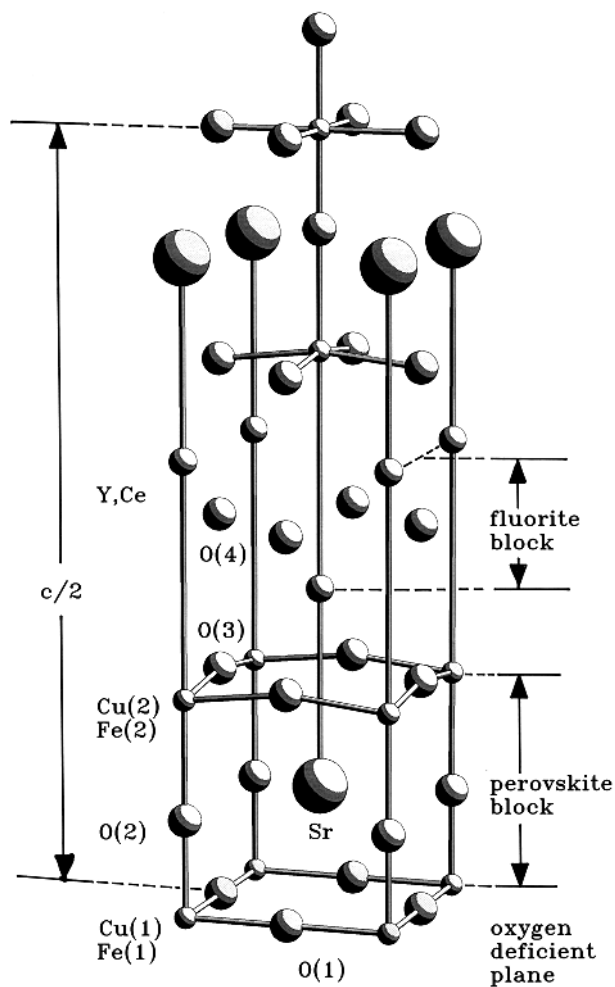∥ Also at: Institute for Crystallography, University of Tübingen, D-72070 Tübingen, Germany.

Figure 1. The crystal structure of the $(Y, Ce)_2Sr_2(Cu, Fe)_3O_{8+y}$ compound.

order as well as the magnetic interactions within and between the Cu(1) and Cu(2) layers. Another issue concerns the exact location of the oxygen atoms in the structure. In this paper we report on the magnetic structure of oxygen-reduced $Y_{1.5}Ce_{0.5}Sr_2Cu_2FeO_{8+y}$ and the crystal structure of oxygen-saturated $Y_{1.5}Ce_{0.5}Sr_2Cu_2FeO_{8+y}$ carried out by means of Rietveld profile refinement of powder neutron diffraction data.

2. Experimental methods

A sample with nominal composition $Y_{1.5}Ce_{0.5}Sr_2Cu_2FeO_{8+y}$ was prepared by thoroughly mixing high-purity stoichiometric amounts of Y_2O_3, CeO_2, $SrCO_3$, CuO and Fe_2O_3. The mixed powders were pelletized, annealed in air at 1120 °C for six days and finally quenched at room temperature (RT) (the *as-prepared sample*—AP). A part of the as-prepared sample was post-annealed at 500 °C under flowing O_2; this treatment was followed by furnace

Table 1. Crystallographic data for the oxygen-saturated (OS) (Y, Ce)$_2$Sr$_2$(Cu, Fe)$_3$O$_{8+y}$ samples obtained using powder neutron diffraction data. Rietveld refinements were carried out using the *I*4/*mmm* (No 139) space group ($Z = 2$). $a = 3.8186(1)$ Å, $c = 28.0749(6)$ Å, $R_p = 4.6$, $R_{wp} = 6.0$, $R_B = 7.6$. N stands for the fractional occupation number for each site and $B = 8\pi^2 \langle U^2 \rangle$ where U is the rms atomic thermal displacement in Å. Anisotropic Bs reflect displacements due to disorder. The numbers in parentheses are estimated standard deviations referred to the last significant digit.

Atom	Wyckoff notation	x	y	z	B	N
Sr	4e	$\frac{1}{2}$	$\frac{1}{2}$	0.0746(2)	$b_{11} = b_{22} = 0.0247$, $b_{33} = 0.0003$	1.0
Y	4e	0	0	0.2966(2)	0.31(1)	0.75
Ce	4e	0	0	0.2966(2)	0.31(1)	0.25
Cu(1)	2a	0	0	0.0	$b_{11} = b_{22} = 0.0112$, $b_{33} = 0.006$	0.5
Fe(1)	2a	0	0	0.0	$b_{11} = b_{22} = 0.0112$, $b_{33} = 0.006$	0.5
Cu(2)	4e	0	0	0.1419(1)	0.80(3)	0.7
Fe(2)	4e	0	0	0.1419(1)	0.80(3)	0.3
O(1)	4c	0	$\frac{1}{2}$	0	$b_{11} = b_{22} = 0.0660$, $b_{33} = 0.0008$	0.64(1)
O(2)	4e	0	0	0.0658(2)	2.8(2)	1.0
O(3)	8g	$\frac{1}{2}$	0	0.1512(1)		1.0
O(4)	4d	$\frac{1}{2}$	0	$\frac{1}{4}$	2.1(2)	1.0

cooling under flowing O$_2$ (the *oxygen-saturated sample*—OS). Finally, another part of the as-prepared sample was post-annealed at 500 °C under flowing Ar for one day and subsequently furnace cooled under flowing Ar (the *oxygen-reduced sample*—OR).

The neutron powder diffraction (NPD) experiments were performed in the flat-cone diffractometer E2 of the research reactor BERII in Berlin. The (311) reflection of the Ge monochromator with wavelength $\lambda = 1.2$ Å and the (002) reflection of the pyrolytic graphite monochromator with wavelength $\lambda = 2.4$ Å were used.

3. Structure refinements

The neutron powder diffraction patterns were refined by Rietveld profile analysis using the FULLPROF program [4], with the peak shapes approximated by a pseudo-Voigt function. The refined parameters were the scale factor, the zero angle, the n-mixing parameter for the Lorentzian and Gaussian components in the pseudo-Voigt function and the unit-cell parameters. For the OR sample, 5 wt.% of the YSr$_2$Cu$_{3-x}$Fe$_x$O$_y$ phase was present and it was included in the refinement as a secondary phase. As a starting model for the refinement we used the structures proposed earlier on the basis of x-ray diffraction data for the OS and OR samples [2]. An idealization of the structure is shown in figure 1. The results of the Rietveld refinement are given in tables 1 and 2. The fitted neutron diffraction patterns are shown in figure 2 for the OS sample (at RT) and in figure 3 for the OR sample ($T = 2$ K). The results of the refinement were similar for the diffractogram of the OR sample at RT. For the OS sample the structural model based on the space group *I*4/*mmm*

Table 2. Crystallographic data for the oxygen-reduced (OR) $(Y, Ce)_2Sr_2(Cu, Fe)_3O_{8+y}$ samples obtained using powder neutron diffraction data. Rietveld refinements were carried out using the $Cmcm$ (No 63) space group ($Z = 2$). $a = 28.376(3)$ Å, $b = 5.432(5)$ Å, $c = 5.431(1)$ Å, $R_p = 4.1$, $R_{wp} = 5.1$, $R_B = 3.4$. N stands for the fractional occupation number for each site and $B = 8\pi^2\langle U^2\rangle$ where U is the rms atomic thermal displacement in Å. The numbers in parentheses are estimated standard deviations referred to the last significant digit.

Atom	Wyckoff notation	x	y	z	B	N
Sr	8g	0.0797(1)	0.7493(2)	0.25	0.6	1.00
Y	8g	0.2953(1)	0.25	0.25	0.4	0.75
Ce	8g	0.2953(1)	0.25	0.25	0.4	0.25
Cu2	8g	0.1422(2)	0.25	0.25	0.3	0.80
Fe2	8g	0.1422(2)	0.25	0.25	0.3	0.20
Cu1	8f	0.0	0.263(3)	0.311(3)	0.1	0.20
Fe1	8f	0.0	0.263(3)	0.311(3)	0.1	0.30
O1	8f	0.0	0.157(3)	0.902(3)	1.3	0.54(5)
O2	16h	0.0632(2)	0.244(3)	0.213(3)	1.0	0.5
O3(1)	8e	0.1511(5)	0.0	0.0	0.4	1.0
O3(2)	8e	0.1495(5)	0.5	0.0	0.7	1.0
O4	8e	0.2524(6)	0.0	0.0	0.5	1.0

was adequate. However, for the OR sample the model based on the $Cmcm$ space group [5] is more appropriate, since it can incorporate the displacement of the ions in the Cu(1) planes. The Bragg factors (R_B) for the OR sample for the $I4/mmm$ and $Cmcm$ space groups were 10% and 3.4% respectively. Consequently, the $Cmcm$ model can be selected on the basis of better agreement factor criteria as well. The octahedral coordination of the (Cu, Fe)(1) cations with oxygen are consistent with the $I4/mmm$ model for the OS sample, in accordance with Mössbauer results. Similarly, for the OR sample the Mössbauer spectra revealed that Fe in the Cu(1) plane appeared most likely to be tetrahedrally coordinated, in agreement with the $Cmcm$ model.

This is in agreement with the neutron powder diffraction experiments performed by Slater and Greaves [6] for $YSr_2Cu_{3-x}M_xO_{7+y}$ (M = Al, Fe, Ti, Pb, Co, Ga) and Harlow *et al* [7] for M^{6+}-substituted $YSr_2Cu_{3-x}M_xO_{7+y}$ (M = Mo, W, Re). These two papers have shown that the chain oxygens were significantly displaced from their $(0, 1/2, 0)$ positions to $(\pm x, 1/2, 0)$ sites on either side of the mirror plane. This means that the substituent atoms induce a cooperative rotational distortion of the chain oxygens, thereby causing a significant departure from the square-planar configuration expected around Cu at this site. The whole situation is consistent with a model in which the (Cu, Fe)(1) atoms are tetrahedrally coordinated. Finally, the occupancies of the O(1) sites for OS and OR samples are estimated to be 64% and 54% respectively.

4. Magnetic structure

Figure 4 shows the neutron diffraction patterns of the OR sample at 2, 50, 150 and 300 K. Close inspection of the neutron diffraction patterns revealed two weak temperature-dependent peaks that could not be accounted for by means of structural refinements. These two peaks were indexed with the superlattice indices $(1/2, 1/2, 2)$ and $(1/2, 1/2, 4)$. Since they are absent from the XRD pattern of the same sample and their intensities decrease with increasing temperature, these peaks can be attributed to magnetic long-range order. For the
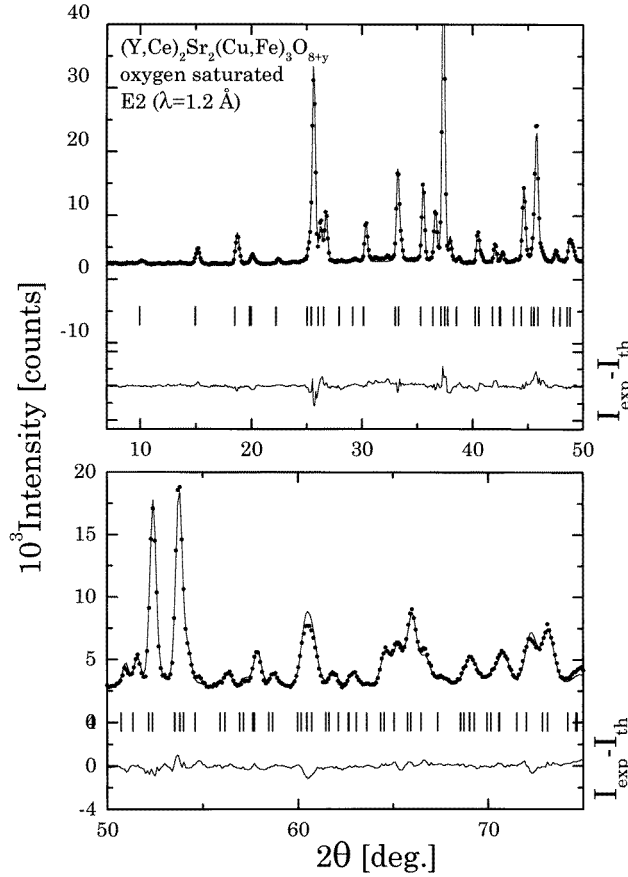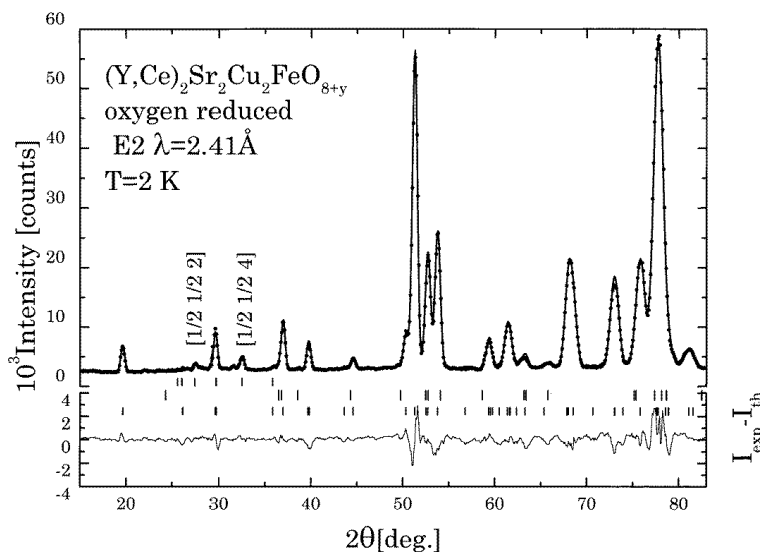
Figure 2. Rietveld refinement patterns at RT for the OS (Y, Ce)$_2$Sr$_2$(Cu, Fe)$_3$O$_{8+y}$ sample obtained using neutron powder diffraction data. The observed intensities are shown by dots and the calculated ones by the solid line. The positions of the Bragg reflections are shown by the small vertical lines below the pattern. The line at the bottom of each panel indicates the intensity difference of the experimental and the refined patterns.

OS sample no magnetic reflection was observed at RT.

These magnetic reflections with indices $(h/2, k/2, l)$ come from a spin arrangement with the propagation vector $\mathbf{k}_1 = [\frac{1}{2}, \frac{1}{2}, 0]$ or $\mathbf{k}_2 = [-\frac{1}{2}, \frac{1}{2}, 0]$. The first two half-integer indices imply that $\mathbf{S}(\mathbf{R} + \mathbf{a}) = -\mathbf{S}(\mathbf{R})$, and $\mathbf{S}(\mathbf{R} + \mathbf{b}) = -\mathbf{S}(\mathbf{R})$, while for the third, $\mathbf{S}(\mathbf{R} + \mathbf{c}) = \mathbf{S}(\mathbf{R})$ (or $\mathbf{S}(\mathbf{R}) = \exp(\mathrm{i}\mathbf{k}_1 \cdot \mathbf{R})\mathbf{S}(\mathbf{0}))$, where $\mathbf{R}$ is a lattice vector and $\mathbf{S}(\mathbf{R})$, $\mathbf{S}(\mathbf{0})$ are the magnetic moments at the lattice sites $\mathbf{R}$ and $\mathbf{0}$, respectively. The integrated intensity of a magnetic reflection for a collinear magnetic structure in a NPD pattern can be written as [8]

$$I(hkl) = \frac{I_0}{v_{0m}^2} \frac{1}{\sin\theta \sin 2\theta} \sum_{\{hkl\}} [1 - (\hat{\mathbf{q}} \cdot \hat{\mathbf{s}})^2] |F(hkl)|^2 \tag{1}$$

where I_0 is the scale factor, v_{0m} is the volume of the magnetic unit cell, θ is the Bragg angle. The summation $\{hkl\}$ must be carried out for all of the equivalent $\{hkl\}$ reflections at the same Bragg angle. $\hat{\mathbf{q}}$ is the unit vector along the direction of the scattering vector, $\hat{\mathbf{s}}$ is the unit vector along the axis of the collinear magnetic structure and $F(hkl)$ is the

Figure 3. Rietveld refinement patterns at 2 K for the OR (Y, Ce)$_2$Sr$_2$(Cu, Fe)$_3$O$_{8+y}$ sample obtained using neutron powder diffraction data (λ = 2.41 Å). The observed intensities are shown by dots and the calculated ones by the solid line. The positions of the Bragg reflections are shown by the small vertical lines below the pattern (bottom to top (Y, Ce)$_2$Sr$_2$Cu$_2$FeO$_{8+y}$, Y$_2$Sr$_2$Cu$_{3-x}$Fe$_x$O$_{6+y}$, magnetic peaks). The line at the bottom indicates the intensity difference of the experimental and the refined patterns. The indices for the magnetic peaks are shown as well.

magnetic structure factor for the configuration symmetry.

For the particular tetragonal crystal structure showing the magnetic structure with the propagation vector k_1, there are two orthorhombic configuration domains with propagation vectors k_1 and k_2. From NPD data for a magnetic structure with orthorhombic configuration symmetry, we can calculate the magnitude of the magnetic moment and the relative orientation of the magnetic moment with respect to the propagation vector [9]. The magnetic structure of the OR compound is similar to the magnetic structures which are observed for the Ln$_2$CuO$_4$ compounds (Ln = rare earths). For example, La$_2$CuO$_4$ displays [10] a magnetic structure with $S \perp k_1$. On the other hand, in Gd$_2$CuO$_4$ [11], the magnetic moment is parallel to k_1 ($S \parallel k_1$). Finally, for Nd$_2$CuO$_4$ both cases are observed [12].

In order to construct a model for the magnetic structure, we supposed that the atom at $(0, 0, 0)$ in the Cu(1) planes has a magnetic moment S_A while that at $(0, 0, z_{Cu(2)})$ in the Cu(2) planes has a magnetic moment S_B. Obviously, the magnetic moments of the ions inside a plane are antiferromagnetically ordered. Since the crystallographic cell is body centred, the magnetic moments are related by a body-centring translation $t = (1/2, 1/2, 1/2)$ given by the relation $S(r + t) = S(r) \exp(ik \cdot t)$. Consequently, the magnetic moments at $(1/2, 1/2, 1/2)$ and $(1/2, 1/2, 1/2 \pm z_{Cu(2)})$ are $-S_A$ and S_B respectively for the propagation vector k_1 and S_A and $-S_B$ for k_2. Another issue is that of whether in the trilayer Cu(2)–Cu(1)–Cu(2) the magnetic moments along the c-axis are antiferromagnetically or ferromagnetically coupled. In view of the above remarks, the possible collinear magnetic models (based on the configuration symmetry) for the propagation vector k_1 are as illustrated in figure 5, with the magnetic moments parallel or perpendicular to the propagation vector.

Thus, the magnetic structure factor for a magnetic unit cell with cell constants

(Y,Ce)$_2$Sr$_2$(Cu,Fe)$_3$O$_{8+y}$ OR
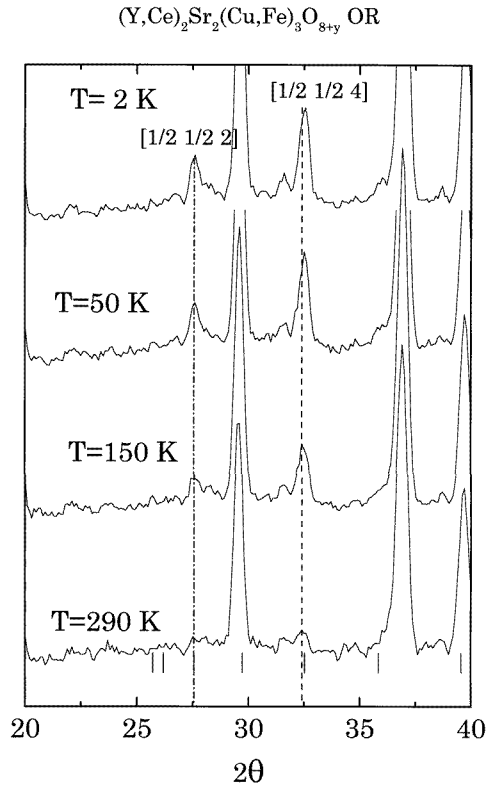
Figure 4. The neutron diffraction patterns of the (Y, Ce)$_2$Sr$_2$(Cu, Fe)$_3$O$_{8+y}$ compound at 2, 50, 150 and 250 K. Only the region with the magnetic peaks is shown.

$a_M = 2a_N$, $b_M = 2b_N$, $c_M = c_N$ and propagation vector k_1 can be written as

$$F(h'k'l') = (1 - e^{\pi i h'})(1 - e^{\pi i k'})$$
$$\times \, [p_A(1 - e^{\pi i l}e^{\pi i(h'+k')/2}) + 2p_B \cos(2\pi l z)(1 - e^{\pi i l}e^{\pi i(h'+k')/2})] \qquad (2)$$

where $p_j = n_j(0.269 \times 10^{-12} \text{ cm}/\mu_B)S_j f_j \exp(-W_j)$, n_j is the occupancy of the jth site, S_j is the average ordered magnetic moment (in Bohr magnetons, μ_B) for the jth site in the jth layer ($j = A, B$), f_j is the magnetic form factor [13] for the magnetic ion in the jth layer and W_j is the Debye–Waller factor for the jth atom. It must be noted that the indices referring to the magnetic unit cell are transformed from $(h/2, k/2, l)$ to (h', k', l) with $h' = 2h, k' = 2k$, but for clarity we prefer to use the half-integers in the discussion of the magnetic structure.

From Mössbauer studies [2] we know that the ordered moments are nearly perpendicular to the c-axis. In such a case the magnetic moment lies within the ab-plane. Since the configuration symmetry is orthorhombic, we can determine the relative orientation of the magnetic moment direction with respect to the propagation vector. Supposing that the magnetic moment is parallel to the propagation vector k_1 (or to the direction [110] in the tetragonal unit cell), the intensity for the $\{(1/2, 1/2, 0)\}$ family of reflections is

$$I' = \sum_{\{110\}}[1 - (\hat{q} \cdot \hat{s})^2]|F(hkl)|^2.$$
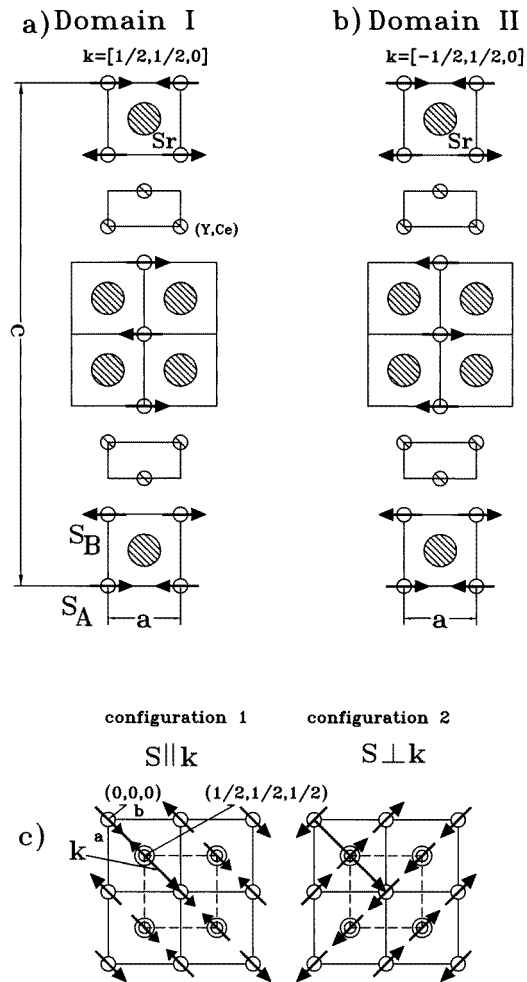
Figure 5. The possible collinear magnetic structures for the $(Y, Ce)_2Sr_2(Cu, Fe)_3O_{8+y}$ compound. There are two domains, (a) domain 1 with propagation vector k_1 and (b) domain 2 with propagation vector k_2. (c) In the first drawing the magnetic moment is parallel to k_1 while in the second one the magnetic moment is perpendicular to k_2.

In view of the orthorhombic configuration symmetry we sum over the $(1/2, 1/2, 0)$, $(-1/2, 1/2, 0)$ and $(1/2, -1/2, 0)$ reflections. The structure factor for the latter two is zero (forbidden), while for the first it is $F(1/2, 1/2, 0) = 8(p_A + 2p_B)$. Within the accuracy of our data the intensity of the $(1/2, 1/2, 0)$ reflection is zero (see figure 4). This fact is compatible with two cases: (a) the magnetic moment being parallel to k_1 ($S \parallel k_1$) and (b) the magnetic moment being perpendicular to k_1 ($S \perp k_1$), and $p_A = -2p_B$ (antiferromagnetic coupling of the magnetic moments inside the trilayer Cu(2)–Cu(1)–Cu(2)). However, if we take into account the other reflections as well, and especially $(1/2, 1/2, 1)$, in order to obtain an agreement between the experimental and calculated intensities, it turns out that the correct option is $S \perp k_1$ and $p_A = -2p_B$. The case with $S \parallel k_1$ and $p_A + 2p_B \neq 0$ gives $I(110) = 0$, but the predicted intensity of $[1/2, 1/2, 1]$ is

larger than the observed one which is approximately zero. The case with $p_A + 2p_B = 0$ and $S \parallel k_1$ must also be excluded because it gives for $(1/2, 1/2, 3)$ an intensity larger than that of $[1/2, 1/2, 4]$ which is the largest observed experimentally. The case with $S \parallel k_2$ and $p_A + 2p_B = 0$ with the spin axis parallel to the propagation vector k_2 also gives the same agreement between the theoretical and calculated intensities. We should note that the magnetic structure can be viewed as a coherent superposition of two configurations ($S \perp k_1$ and $S \parallel k_2$). This degeneracy is a familiar problem [14] in magnetic structure analysis based on neutron powder diffraction data and is difficult to resolve without a single crystal which is predominantly of one-domain form. At this point we should mention that the compound (Y, Ce)$_2$Sr$_2$CuFeO$_8$ (which is isostructural with Nd$_2$CuO$_4$) has the same structure as (Y, Ce)$_2$Sr$_2$(Cu, Fe)$_3$O$_{8+y}$, except for the absence of Cu(2) planes, and displays a magnetic peak [15] at $(1/2, 1/2, 0)$. In other words, $S \perp k_1$ and $S_A \neq 0$.

Since we have a large number of parameters and a small number of magnetic reflections,
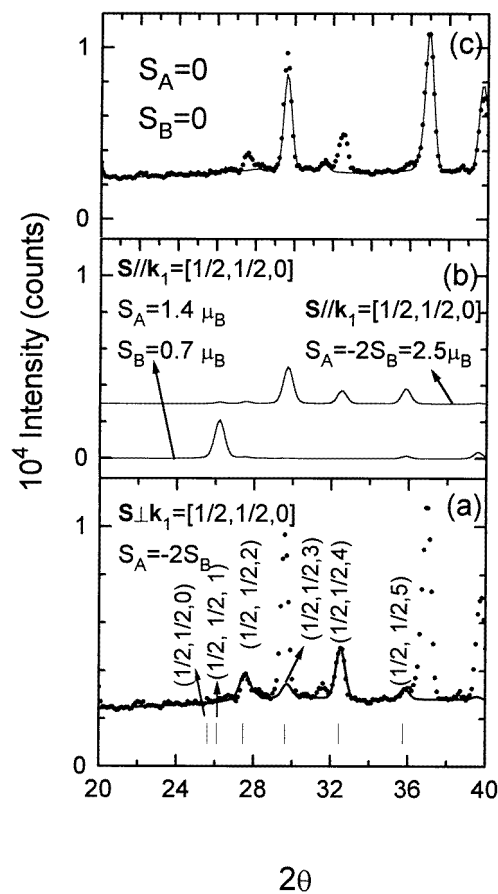
Figure 6. Calculated neutron diffraction patterns for the magnetic reflections of the OR (Y, Ce)$_2$Sr$_2$(Cu, Fe)$_3$O$_{8+y}$ compound as a function of the moment at the Cu(1) sites and the relative directions of the spin and k_1. The experimental patterns fit better when $S_A = -2S_B$ and $\hat{s} \perp k_1$ (a). In the other two cases with $\hat{s} \parallel k_1$, regardless of the relationship between S_A and S_B, the agreement is rather poor (b). Panel (c) shows the intensity contribution from the crystal structure.

it would be difficult to consider two kinds of magnetic ion, each one having a different moment. For this reason we assumed that the magnetic ions are represented by a mean magnetic moment. On the other hand, we should note that there might be an error in the estimation of the mean magnetic moment, but the small contribution of the Cu^{2+} moment would not appreciably alter the final result. We used the FULLPROF program to test all of the above-mentioned magnetic structure models and estimate S_A and S_B. This procedure gave the best agreement between the theoretical and calculated intensities for configuration 2 ($\hat{s} \perp k_1$) and the constraint $S_A = -2S_B$. Figure 6(a) clearly shows the aforementioned agreement, whereas when S is parallel to k_1, regardless of the relationship between S_A and S_B, the agreement is obviously not acceptable. The ordered magnetic moments per ion at 2 K were estimated to be $S_A = (-1.04(2) \mu_B, 1.04(2) \mu_B, 0)$ ($S_A = 1.47 \pm 0.02 \mu_B$) and $S_B = (0.52(2) \mu_B, -0.52(2) \mu_B, 0)$ ($S_B = 0.73 \pm 0.02 \mu_B$). The same analysis, when applied at 150 and 300 K, yields $S_B = 0.58 \pm 0.02 \mu_B$, $S_A = 0.87 \pm 0.02 \mu_B$ and $S_A = 0.56 \pm 0.05 \mu_B$, $S_B \simeq 0.28 \pm 0.02 \mu_B$, respectively.

Finally, let us discuss the values of the ordered moments at 2 K in comparison to the Mössbauer and susceptibility results [2]. The average ordered magnetic moment per ion at 2 K for the Cu(2) and Cu(1) sites was found to be $S_A = 1.47(2) \mu_B$ and $S_B = 0.73(2) \mu_B$. According to the results from the MS for the same compounds, the distribution of iron and copper at the Cu(1) and Cu(2) sites is $[(0.55Fe + 0.45Cu)_1, (0.775Cu + 0.225Fe)_2]$. Consequently, if we supposed that Cu^{2+}, $Fe(1)^{3+}$ and $Fe(2)^{3+}$ have magnetic moments ($\mu = g\mu_B J$) of approximately 1, 3 and 5 μ_B respectively, then the average moments at zero temperature would be $S_A = 2.1 \mu_B$ and $S_B = 1.9 \mu_B$. However, it is well known (see Casalta *et al* [16]) that the Cu ordered magnetic moment in $YBa_2Cu_3O_6$ at 0 K is not 1 μ_B but only $\sim 0.55 \mu_B$ (due to quantum spin fluctuations and the covalence of the $3d_{x^2-y^2}$ orbital of the Cu(2) with neighbouring oxygen 2p orbitals). From magnetization measurements and Mössbauer data we have strong evidence that a small fraction of iron (at Cu(1) sites) and Cu exists in both statically and/or dynamically disordered states as well as in ordered ones.

5. Conclusions

The structure of the $(Y, Ce)_2Sr_2(Cu, Fe)_3O_{8+y}$ compound was refined on the basis of the $I4/mmm$ and $Cmcm$ space groups for OS and OR samples respectively. For the OR sample we observed magnetic reflections with indices $[\frac{1}{2}\frac{1}{2}l]$. The magnetic structure is realized by an antiferromagnetic arrangement inside each layer and inside each trilayer as well. The observed intensities indicate that both the Cu(1) layers and the Cu(2) layers have non-zero magnetic moments.

Acknowledgments

References

[1] Wada T, Nare A, Ichinose A, Yamauchi H and Tanaka S 1992 *Physica* C **192** 181
[2] Pissas M, Kallias G, Poulakis N, Niarchos D, Simopoulos A and Liarokapis E 1995 *Phys. Rev.* B **52** 10 610
[3] Felner I, Schmitt D and Barbara B 1997 *Physica* B **229** 153

[4] Rodriguez-Carvajal J 1990 FULLPROF: a program for Rietveld refinement and pattern matching analysis
       Satellite Mtg on Powder Diffraction of the 15th Congr. of the IUCr (Toulouse) abstracts, p 127
       Rodriguez-Carvajal J 1993 *Physica* B **192** 55
[5] Wright A J and Greaves C 1994 *Physica* C **235–240** 885
[6] Slater P R and Greaves C 1991 *Physica* C **180** 299
[7] Harlow R L, Kwei G H, Suryanarayanan R and Subramanian M A 1996 *Physica* C **257** 125
[8] Rossat-Mignod J 1987 *Methods of Experimental Physics* (New York: Academic) p 69
[9] Shirane G 1959 *Acta Crystallogr.* **12** 282
[10] Vaknin D *et al* 1987 *Phys. Rev. Lett.* **58** 2802
[11] Chattopadhyay T *et al* 1992 *Phys. Rev.* B **46** 5731
[12] Skanthakumar S *et al* 1989 *Physica* C **160** 124
       Endoh Y *et al* 1989 *Phys. Rev.* B **40** 7023
       Freltoft T *et al* 1991 *Phys. Rev.* B **44** 5046
       Matsuda M *et al* 1990 *Phys. Rev.* B **42** 10 098
[13] Watson R E and Freeman A J 1961 *Acta Crystallogr.* **14** 27
[14] Cox D E *et al* 1989 *Phys. Rev.* B **40** 6998
[15] Pissas M 1998 *BENSC Experimental Report*
[16] Casalta H *et al* 1994 *Phys. Rev.* B **50** 9688